Geophysical Journal International

Geophys. J. Int. (2024) **238,** 848–859
Advance Access publication 2024 June 05
GJI Gravity, Geodesy and Tides

https://doi.org/10.1093/gji/ggae196

Subsurface tidal gravity variation and gravimetric factor

Y. Rogister [1], J. Hinderer,[1] U. Riccardi [2] and S. Rosat [1]

[1] *Institut Terre et Environnement de Strasbourg, Université de Strasbourg/EOST, UMR 7063, CNRS, 67000 Strasbourg, France. E-mail: yves.rogister@unistra.fr*
[2] *Dipartimento di Scienze della Terra, dell'Ambiente e delle Risorse (DiSTAR), University "Federico II" of Napoli, 80126 Napoli, Italy*

Accepted 2024 May 28. Received 2024 May 3; in original form 2023 December 20

SUMMARY

Taking advantage of the simultaneous recording during 471 d between 2019 and 2021 by two superconducting gravimeters installed at the surface and 520 m under the surface at the Low Noise Underground Laboratory (LSBB) in Rustrel, France, we investigate whether a difference between the tidal gravity signals at the two locations can be detected. First, we model the periodical variations of the Earth's gravity owing to the tidal influence from the Sun and Moon, at the Earth's surface and at shallow depths. We provide analytical formulae for the Love numbers, gravimetric factor and gravity variation of simple spherical planetary models. We also numerically compute those parameters and function for a realistic spherical Earth model. We find that the fractional difference between the semi-diurnal tidal gravity variations at the surface and 520 m below is as small as 8.5×10^{-5}. We next evaluate the effect on the amplitude of the recorded gravity signal due to the calibration factors of the two superconducting gravimeters at LSBB. Finally, we compute the spectra of the difference between the gravity variations measured on and under the surface in the semi-diurnal band of the M_2 tidal wave. We find that the uncertainties associated to the calibration factors are larger than the theoretical or observational difference between the tidal gravity variations on the surface and at a 520-m depth.

Key words: Time variable gravity.

1 INTRODUCTION

The body and ocean tides generated by the Sun, the Moon and, to a lesser extent, by other celestial bodies, are the causes of the largest periodical gravity variations on Earth. Body tides, which are planetary scale, are very well understood from a theoretical point of view, which involves both celestial mechanics and geophysics. Their accurate prediction requires the knowledge of the positions of the Sun and the Moon and of the orientation of the Earth in space, as well as the modelling of the global elasto-gravitational deformation of the Earth. In the following, we will only be interested in the geophysical side of the phenomenon. We refer the reader to Wilhelm *et al.* (1997) for a selection of references on this topic.

Often involved in studies of the tidal gravity variations is the gravimetric factor, which is a dimensionless number defined at the surface of the Earth. According to the recommendations of the Working Group on the Theoretical Tidal Model (Special Study Group of the Earth Tide Commission Sec. V of the International Association of Geodesy), the gravimetric factor is defined as the Earth's transfer function between the body tide signal measured at the station by a gravimeter and the amplitude of the vertical component of the gradient of the external tidal potential at the station. From a theoretical point of view, the Earth model being assumed spherically symmetric, both the small disturbing force and the resulting small gravity variation are expanded in vector spherical harmonics, so that a disturbing force of harmonic degree ℓ causes a gravity variation of the same degree. Moreover the corresponding gravimetric factor is of the same degree and shall be denoted by δ_ℓ.

The classical derivation of the linearized analytical expression for δ_ℓ is based on the decomposition of the Lagrangian gravity variation at a point in a sum of three terms. The first term comes from the perturbing force itself, in our case the tidal force. The second term comes from the displacement of the mass point in the initial surrounding Earth's self-gravity field. And the third term comes from the Eulerian variation of the Earth's self-gravity. The second and third terms are proportional to Love (1909) numbers. The derivation can be found in Wahr (1981) or Hinderer & Legros (1989). We however rederive the expression for the gravimetric factor in Section 2. Because the density and the particle displacement are discontinuous across the surface, so are both the gradient of the initial gravity and the Eulerian variation of the gravity potential. Care must then be taken in distinguishing the definition of the gravimetric factor by approaching the surface from above or from below. Since the gravimetric factor can be expressed in terms of Love numbers, we derive original formulas for the degree-2 dynamic Love numbers of homogeneous and incompressible models, fluid or solid. Although of no

much use nowadays in geophysics, such simple models are of interest in planetary science (for instance, Rambaux & Castillo-Rogez 2013; Peale & Canup 2015; Bierson 2024).

In Section 3, which is the core of the theoretical part of the paper, we analytically and numerically investigate the tidal gravity variation as a function of depth for different Earth models. A motivation to develop a theory of subsurface tidal gravity variation is that available softwares for tidal analysis, such as ETERNA-X (Schüller 2020), only handle gravity measurements at the surface of the Earth. They do not allow for a tidal analysis of the data recorded at a station under the ground. In view of the subsequent analysis of observational data acquired with superconducting gravimeters on the surface and under the surface (Sections 4 and 5), we limit our computations to semi-diurnal tides at depths smaller than 1 km. The results would not be significantly different for other periods of the forcing, for instance for ter-diurnal or diurnal periods. The Love numbers and gravimetric factor would abruptly change in case of resonance, that is if the frequency of the forcing was close to the frequency of a normal mode. But there are no nearly semi-diurnal or ter-diurnal modes, either computed for realistic Earth models or observed. Our homogeneous Earth models do not have semi-diurnal or ter-diurnal modes either. The Free Core Nutation and Free Inner Core Nutation are rotational nearly diurnal normal modes of rotating elliptical Earth models. They do not matter for the theory developed in the paper since we only consider non-rotating spherical Earth models. There are no known long-period normal modes, except the Chandler wobble that, anyway, is not a resonant mode because its period is not close to a tidal period. Moreover, spherical non-rotating models have no Chandler wobble. We could speculate on the existence, theoretical or observational, of long-period inertia-gravity modes confined to the liquid core. But, having most of their energy in the deep Earth, they would not much influence the tidal deformation in the crust.

Besides, from gravity data, a software like ETERNA-X derives, among other things, the amplitude and phase of the gravimetric factor for separate sets of tidal waves that have close frequencies. Therefore, to provide a consistent presentation to the reader familiar with ETERNA-X or similar programs, we also search to determine whether the expression for the gravimetric factor in terms of Love numbers can be generalized downward to small depths.

First measurements of tidal gravity variations were made by Schweydar in Potsdam, Germany, in 1914 (Torge 1989). From the middle of the 20th century, long-term observations with spring gravimeters developed (see Calvo [2015] for a brief historical account). In the 1980s, superconducting gravimeters became commercially available. They are today the most stable and most sensitive relative gravimeters (Hinderer *et al.* 2015).

In this paper, we focus on the difference between the gravity signals simultaneously recorded during 471 d between 2019 and 2021 by two superconducting gravimeters on the surface and at a 520-m depth at the Low Noise Underground Laboratory (LSSB = Laboratoire Souterrain à Bas Bruit, https://lsbb.cnrs.fr/) in Rustrel, France. Their location at LSBB is shown in Fig. 1, emphasizing the 520-m height difference. The surface instrument iGrav31 was installed in 2019 May in the framework of the CRITEX project, which aims at studying the critical zone (https://www.critex.fr). The underground instrument iOSG24 is part of the MIGA experiment (first laser-based atom interferometer for gravitational wave detection, http://miga-project.org). It was installed in 2016 (Rosat *et al.* 2018).

In Section 4, we estimate the calibration factors of the gravimeters. In Section 5, we process the data sets from the two instruments in a similar way over a common duration and investigate the difference between the tidal signals. Finally, in Section 6, we draw the conclusion about this study.

2 TIDAL GRAVITY VARIATION, LOVE NUMBERS AND GRAVIMETRIC FACTOR

We consider an unperturbed self-gravitating non-rotating Earth model in hydrostatic equilibrium. It is therefore spherically symmetric. If we denote by $\mathbf{r}$ the position vector whose origin is at the centre of mass, which is the centre of the sphere, gravity $\mathbf{g}$ at $\mathbf{r}$ derives from gravitational potential $\phi(\mathbf{r})$:

$$\mathbf{g}(\mathbf{r}) = -g(r)\frac{\mathbf{r}}{r} = -\nabla\phi(r), \tag{1}$$

where ∇ is the gradient operator. Because there cannot be two material particles simultaneously at the same geometrical position, the mass point initially located at space point $\mathbf{r}$ is also called $\mathbf{r}$.

The Earth is then perturbed by a periodic tidal force which is the opposite of the product of the density and the gradient of tidal potential $\phi_T(\mathbf{r},\ \omega)$, where ω is the angular frequency of the oscillation. The displacement vector of mass point $\mathbf{r}$ is $\mathbf{u}(\mathbf{r},\ \omega)$. The time variation of the gravitational potential at a geometrical location is called Eulerian variation of ϕ and is denoted by $\phi^\Delta(\mathbf{r},\ \omega)$. The time variation of gravity following a mass point in its displacement is called Lagrangian variation of $\mathbf{g}$ and is denoted by $\mathbf{g}^\delta(\mathbf{r},\ \omega)$. To the first order in $\mathbf{u}$, $\mathbf{g}^\delta$ and ϕ^Δ, which are assumed to be small, we have (Dahlen & Tromp 1998)

$$\mathbf{g}^\delta = -\nabla\phi_T + (\mathbf{u}\cdot\nabla)\mathbf{g} - \nabla\phi^\Delta. \tag{2}$$

Therefore, the radial component of $\mathbf{g}^\delta$ is

$$g_r^\delta = -\phi_T' - u_r g' - \phi^{\Delta'}, \tag{3}$$

where u_r is the radial displacement and the prime denotes the radial derivative. It should be stressed that relations (2) and (3) are, theoretically, valid where $\mathbf{g}$, $\mathbf{u}$, $\mathbf{g}^\delta$, ϕ^Δ and ϕ_T are defined, which is inside the Earth. Outside the Earth, $\mathbf{g}$, ϕ_T and ϕ^Δ are well defined but $\mathbf{g}^\delta$ and $\mathbf{u}$ are not because there is no material particle.

We then decompose the scalar functions ϕ^Δ, u_r and ϕ_T in series of fully normalized spherical harmonics $Y_\ell^m(\theta,\ \varphi)$, θ and φ being the colatitude and longitude, respectively:

$$\phi^\Delta(r,\ \theta,\ \varphi,\ \omega) = \sum_{\ell=0}^{\infty}\sum_{m=-\ell}^{\ell} {\phi^\Delta}_\ell^m(r,\ \omega)\, Y_\ell^m(\theta,\ \varphi), \tag{4}$$

$$u_r(r,\ \theta,\ \varphi,\ \omega) = \sum_{\ell=0}^{\infty}\sum_{m=-\ell}^{\ell} {u_r}_\ell^m(r,\ \omega)\, Y_\ell^m(\theta,\ \varphi), \tag{5}$$

$$\phi_T(r,\ \theta,\ \varphi,\ \omega) = \sum_{\ell=0}^{\infty}\sum_{m=-\ell}^{\ell} {\phi_T}_\ell^m(r,\ \omega)\, Y_\ell^m(\theta,\ \varphi). \tag{6}$$

To simplify the notations, we drop subscript ℓ and superscript m from ${\phi^\Delta}_\ell^m$, ${u_r}_\ell^m$ and ${\phi_T}_\ell^m$, as well as the explicit dependence on ω. So, we simply write that $\phi_T(r)$ varies as r^ℓ (Wenzel 1997):

$$\phi_T(r) \sim r^\ell \tag{7}$$

for any r.

We are interested in evaluating g_r^δ at the surface $r = a$ of the Earth and 520 m under the surface. However, evaluating g_r^δ at the surface $r = a$ poses a problem because g' and $\phi^{\Delta'}$ are discontinuous there (see boundary conditions [11] and [13] below). We now address this issue.

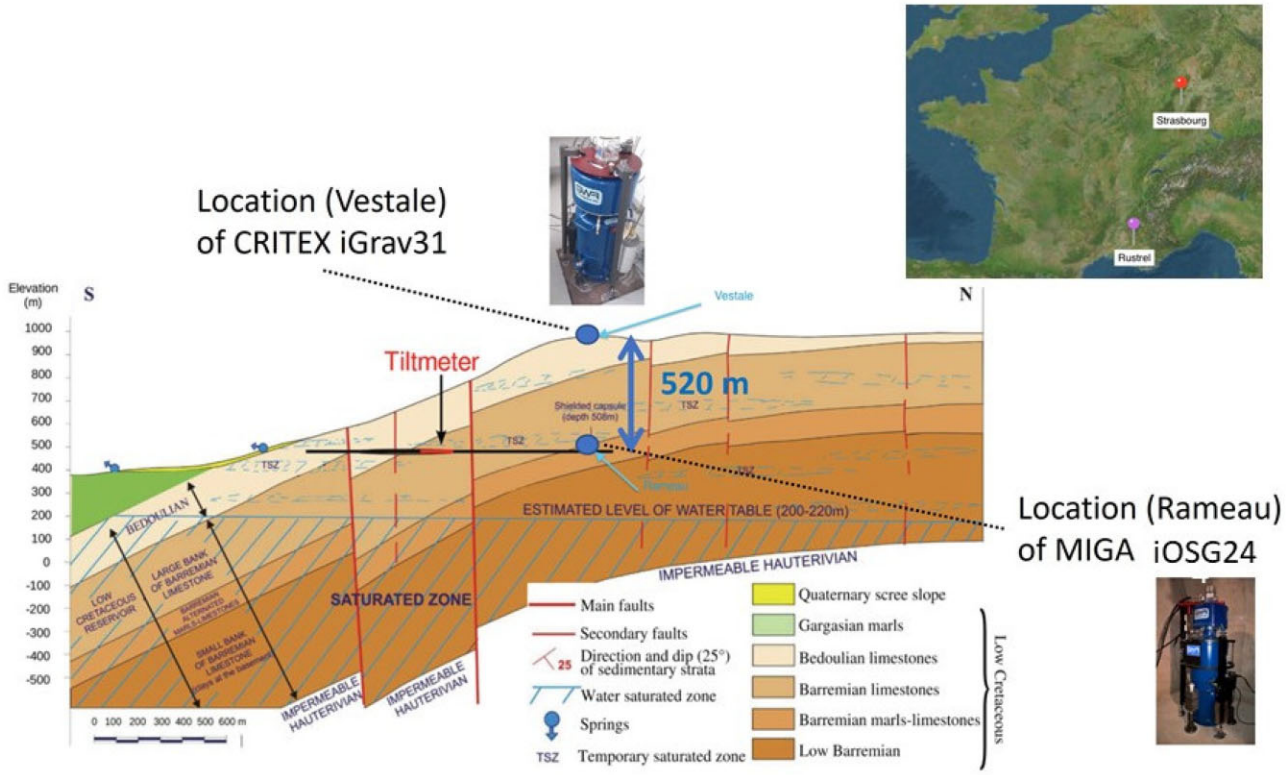

Figure 1. Superconducting gravimeters iGrav31 and iOSG24 vertically distant by 520 m at the LSBB site in Rustrel, France (modified from Sénéchal *et al.* 2013). The hydrological catchment is in a karstic context with an estimated water table lower than the iOSG24 location in a tunnel. Upper right corner inset: location of Rustrel and Strasbourg. The geographical coordinates of the iGrav31 are 43°56′28.13741″ N, 5°29′1.42274″ E and those of the iGrav31 are 43°56′30.00080″ N, 5°29′4.70715″ E. The iGrav31 was also calibrated at the station J9 (48.622°N, 7.684°E) approximately 10 km northwest of Strasbourg (Section 4).

Let us respectively denote by f_+ and f_- the limits

$$f_+ = \lim_{r \searrow a} f(r) \tag{8}$$

and

$$f_- = \lim_{r \nearrow a} f(r) \tag{9}$$

of the function $f(r)$ at $r = a$. The surface $r = a$ being a discontinuity boundary for the density ρ, we have the following boundary conditions (Kellogg 1953; Alterman *et al.* 1959):

$$g_+ - g_- = 0, \tag{10}$$

$$g'_+ - g'_- = -4\pi G\rho_-, \tag{11}$$

$$\phi^{\Delta}_+ - \phi^{\Delta}_- = 0, \tag{12}$$

$$\phi^{\Delta'}_+ - \phi^{\Delta'}_- = 4\pi G\rho_- u_{r-}, \tag{13}$$

$$\phi_{T+} - \phi_{T-} = 0, \tag{14}$$

$$\phi'_{T+} - \phi'_{T-} = 0, \tag{15}$$

where G is the gravitational constant. Boundary conditions (10) and (11) are associated to Poisson's equation for ϕ inside the Earth

$$\nabla^2\phi^{\text{in}} = -\nabla\cdot\mathbf{g}^{\text{in}} = 4\pi G\rho \qquad \text{for } r < a, \tag{16}$$

where ∇^2 and $\nabla\cdot$ are the Laplace and divergence operators, respectively, and Laplace's equation for ϕ outside the Earth

$$\nabla^2\phi^{\text{out}} = -\nabla\cdot\mathbf{g}^{\text{out}} = 0 \qquad \text{for } r > a. \tag{17}$$

Boundary conditions (12) and (13) are associated to Poisson's equation for ϕ^{Δ} inside the Earth

$$\nabla^2\phi^{\Delta\,\text{in}} = -4\pi G\nabla\cdot(\rho\mathbf{u}) \qquad \text{for } r < a \tag{18}$$

and Laplace's equation for ϕ^{Δ} outside the Earth

$$\nabla^2\phi^{\Delta\,\text{out}} = 0 \qquad \text{for } r > a. \tag{19}$$

We ascribe the displacement u_{r-} to the material particles initially at $r = a$. So, we can write

$$u_r(a) = u_{r-}. \tag{20}$$

Whereas g^{δ}_{r-} is well defined, it does not make sense to speak of $\mathbf{g}^{\delta}$ outside the Earth because there is no particle to move with. Nevertheless, we define g^{δ}_{r+} as follows:

$$g^{\delta}_{r+} = -\phi^{\Delta'}_+ - u_{r-}g'_+ - \phi'_{T+}. \tag{21}$$

This is justified by the experimental setup (Wahr 1981). Indeed, the support of a superconducting gravimeter (Hinderer *et al.* 2015), for instance, is rigidly connected to the surface and simultaneously moves with it. Therefore, we used u_{r-} in formula (21). Inside the instrument, a levitated sphere is maintained at rest by a magnetic force that exactly compensates the gravity forces exerted by the Earth, Sun and Moon and the inertia force due to the motion of

the instrument with the surface. Neglecting the inertia force, measurements of the variations of the applied magnetic force allows for estimating the gravity variations. The levitated sphere is maintained above the surface, that is in the exterior Earth's gravity field, explaining why we used g'_+, $\phi^{\Delta'}_+$ and ϕ'_{T+} in relation (21).

As a consequence of the definition (21) and relations (11)–(15), we have

$$g^\delta_{r+} = g^\delta_{r-}, \tag{22}$$

which is the Lagrangian gravity variation $g^\delta_r(a)$ we ascribe to the surface. Consequently, this last relation and relation (21) are the solution to the problem raised above about the evaluation of the tidal gravity variation at the surface of the model.

Taking advantage of the linearity of the equations of motion and of the spherical symmetry of the Earth model, one defines dimensionless functions $H_\ell(r)$ and $K_\ell(r)$ independent of m and of the forcing by (Love 1909)

$$u_r(r) = -H_\ell(r)\frac{\phi_T(r)}{g(r)}, \tag{23}$$

$$\phi^\Delta(r) = K_\ell(r)\phi_T(r). \tag{24}$$

Similarly to the functions $H_\ell(r)$ and $K_\ell(r)$ that are related to the particle displacement and Eulerian gravitational potential variation, respectively, we define the dimensionless function $\Delta_\ell(r)$ related to the Lagrangian variation of gravity by:

$$\Delta_\ell(r) = -\frac{g^\delta_r(r)}{\phi'_T(r)}. \tag{25}$$

In particular, at the surface $r = a$ of the spherical model, $H_\ell(a)$ and $K_\ell(a)$ are the tidal Love numbers h_ℓ and k_ℓ (Love 1909)

$$h_\ell = H_\ell(a), \tag{26}$$

$$k_\ell = K_\ell(a) \tag{27}$$

and $\Delta_\ell(a)$ is the gravimetric factor δ_ℓ

$$\delta_\ell = \Delta_\ell(a). \tag{28}$$

Given eqs (22) and (25), δ_ℓ can be calculated by using either g^δ_{r+}, defined by formula (21), or g^δ_{r-}, obtained by letting r increase towards a in eq. (3). The usual derivation of δ_ℓ in terms of the Love numbers relies on formulae (21) and (23)–(28) (for instance, Wahr 1981; Hinderer & Legros 1989). For $r > a$, the gravity g^{out} outside a spherically symmetrical body of mass M is proportional to r^{-2} :

$$g^{\text{out}}(r) = \frac{GM}{r^2} \tag{29}$$

and $\phi^{\Delta\,\text{out}}$ is proportional to $r^{-(\ell+1)}$ for a given degree ℓ

$$\phi^{\Delta\,\text{out}}(r) \sim r^{-(\ell+1)} \tag{30}$$

because it is solution of Laplace's eq. (19). Consequently, for any $\ell \neq 0$, we have

$$\delta_\ell = 1 + \frac{2}{\ell}h_\ell - \frac{\ell+1}{\ell}k_\ell. \tag{31}$$

In particular, for $\ell = 2$, which is the case of semi-diurnal tides, we obtain

$$\delta_2 = 1 + h_2 - \frac{3}{2}k_2. \tag{32}$$

In the next section, we calculate the tidal variation of gravity under the surface.

3 SUBSURFACE TIDAL GRAVITY VARIATIONS

To evaluate g^δ_{r+}, defined by eq. (21), we needed analytical expressions for g and ϕ^Δ outside the Earth. Of course, to evaluate g^δ_r by approaching the Earth's surface from the inside, that is g^δ_{r-}, we would need analytical expressions for g and ϕ^Δ inside the Earth. However, one or the other, or both, are generally not known analytically inside realistic Earth models. We therefore turn either to simple Earth models for which g^{in} and $\phi^{\Delta\,\text{in}}$ can be determined analytically, or to numerical computation for a realistic Earth model.

First, let us consider an incompressible homogeneous Earth model, be it solid or liquid. Self-gravity inside the unperturbed model is

$$g^{\text{in}}(r) = \frac{4\pi}{3}G\rho r\ , \tag{33}$$

where ρ is the constant density. Moreover, the Eulerian variation of the potential $\phi^{\Delta\,\text{in}}$ is proportional to r^ℓ because it is a solution of Laplace's equation

$$\nabla^2\phi^{\Delta\,\text{in}} = 0 \tag{34}$$

when the material is both homogeneous and incompressible:

$$\phi^{\Delta\,\text{in}}(r) \sim r^\ell. \tag{35}$$

Consequently, for any $\ell \neq 0$, we obtain

$$\delta_\ell = 1 - \frac{1}{\ell}h_\ell + k_\ell \tag{36}$$

by inserting g^δ_{r-} in $\Delta_\ell(a)$ in eq. (28). The comparison between eqs (31) and (36) provides a relation between the Love numbers h_ℓ and k_ℓ:

$$k_\ell = \frac{3}{2\ell+1}h_\ell, \tag{37}$$

then a relation between the gravimetric factor δ_ℓ and the Love number h_ℓ:

$$\delta_\ell = 1 + \frac{2(\ell-1)}{\ell(2\ell+1)}h_\ell. \tag{38}$$

We insist that the last two relations only hold true for incompressible homogeneous models. In particular, for $\ell = 2$, we obtain

$$k_2 = \frac{3}{5}h_2 \tag{39}$$

and

$$\delta_2 = 1 + \frac{h_2}{10}. \tag{40}$$

In Appendix A, we show that, if the model is fluid, the Love number h_2 is

$$h_2 = \frac{10}{4 - 5\mathfrak{m}}, \tag{41}$$

where $\mathfrak{m}$ is the dimensionless parameter defined by

$$\mathfrak{m} = \frac{\omega^2 a}{g(a)}. \tag{42}$$

If the model is solid, we have, to a good approximation,

$$h_2 \simeq \frac{5}{2}\left\{1 + \frac{19\mu}{2\rho g(a)a}\left[1 - \frac{79}{570}x^2(a) - \frac{143}{410400}x^4(a)\right]\right\}^{-1}, \tag{43}$$

where

$$x = x(r) = \kappa r, \tag{44}$$

Table 1. For the M_2 period of 12h25m14s and a slightly modified version of PREM, tidal potential, its radial derivative and other quantities listed in the first column, and defined in the text, at the surface (second column) and at a 520-m depth (third column). The degree-2 harmonic component of the lunar tidal potential ϕ_T is $GM_{\mathbb{C}}\, r^2/D_{\mathbb{C}}^3$, where $M_{\mathbb{C}} = 7.349\ 10^{22}$ kg is the mass of the moon and $D_{\mathbb{C}} = 3.844\ 10^8$ m is the mean Earth–moon distance.

	$r = a = 6371$ km	$r = 6370.48$ km
ϕ_T (m^2 s^{-2})	3.5044062	3.5038342
ϕ_T' (10^{-6} m s^{-2})	1.1001118	1.1000220
g (m s^{-2})	9.8239685	9.8244386
g'_- (10^{-7} s^{-2})	−9.0372421	–
g'_+ (10^{-7} s^{-2})	−30.8396437	–
g' (10^{-7} s^{-2})	–	−9.0412351
u_r (m)	−0.2190984	−0.2191067
H_2	$h_2 = 0.6142029$	0.6143555
ϕ^Δ (m^2 s^{-2})	1.0649805	1.0649929
$\phi_-^{\Delta'}$ (10^{-8} m s^{-2})	−2.3794623	–
$\phi^{\Delta'}$ (10^{-8} m s^{-2})	–	−2.3907717
K_2	$k_2 = 0.30389754$	0.3039507
g_r^δ (10^{-6} m s^{-2})	−1.2743218	−1.2742138
Δ_2	$\delta_2 = 1.1583566$	1.1583530
$1 + H_2 - 3K_2/2$	$\delta_2 = 1 + h_2 - -3k_2/2 = 1.1583566$	1.1584294

$$\kappa^2 = \frac{\rho\omega^2}{\mu} \tag{45}$$

and μ is rigidity.

We take $\rho = 5515$ kg m^{-3} and $a = 6371$ km, hence $g(a) = 9.82$ m s^{-2}. At the M_2 tidal period, which is 12h25m14s, we find $\mathfrak{m} = 1.2807\ 10^{-2}$, $h_2 = 2.5407$, $k_2 = 1.5244$ and $\delta_2 = 1.2541$ for a fluid sphere. If, moreover, we take $\mu = 1.46 \times 10^{11}$ Pa, we find $h_2 = 0.4998$, $k_2 = 0.299$ and $\delta_2 = 1.04998$ for a solid sphere.

Because we assumed the Earth model to be a homogeneous and incompressible sphere when we derived $g_{r\,-}^\delta$, eqs (33)–(40) are not valid anymore for realistic Earth models, which are compressible, inhomogeneous, partially solid and partially liquid. We consider the PREM model (Preliminary Reference Earth Model, Dziewonski & Anderson 1981) where we replace the global ocean by a 3-km thick extension of the upper crust. We numerically integrate the equations of motion (Alterman *et al.* 1959) at the M_2 period and obtain the results displayed in the second column of Table 1.

Let us next have a look at the function $\Delta_\ell(r)$, defined by relation (25), inside the Earth. Actually, we would like to know whether relation (31) can also be used inside the Earth, close to the surface, as an approximation to $\Delta_\ell(r)$, provided, of course, h_ℓ and k_ℓ be replaced by $H_\ell(r)$ and $K_\ell(r)$, respectively.

Again, we consider a simple homogeneous incompressible Earth model. Let us assume it is fluid. Taking into account eqs (7), (33) and (35) and eq. (A1), we find that the Lagrangian gravity variation g_r^δ varies as $r^{\ell-1}$. For $\ell = 2$, it is a linear function of r so that the fractional variation of g_r^δ between the surface and depth $d \ll a$ is d/a, which is $8.16\ 10^{-5}$ for $d = 520$ m. As for $\Delta_\ell(r)$ defined by relation (25), it is actually depth independent and is given by eq. (A6).

Let us next consider a solid model. We show in Appendix A that the radial displacement $u_r(r)$ is not a linear function of r. Therefore $g_r^\delta(r)$ is not a linear function of r either and $\Delta_\ell(r)$ is not constant. However, the differences between, respectively, g_r^δ and the degree-2 gravimetric factor at $r = a$ and at $r = a - d$ are 0.12 nm s^{-2} and 2.5×10^{-5} only. The fractional difference between the values of g_r^δ at the surface and at a 520-m depth is 10^{-4}, barely more than in the liquid case.

Again by lack of analytical solution for the tidal deformation of realistic Earth models, we have to rely on the numerical computation of the tidal gravity variation inside them. So, for our modified version of PREM, we obtain the third column of Table 1, which gives the values of various quantities at a 520-m depth. We see that the semi-diurnal tidal gravity variation g_r^δ is bigger by 0.11 nm s^{-2} at the surface than under the surface. Consequently, the fractional difference between the values of g_r^δ at the surface and at a 520-m depth is 8.47×10^{-5}, which is close to what we found for our simple fluid Earth model right above. Moreover, the difference at a 520-m depth between $1 + H_2 - 3K_2/2$ and Δ_2 amounts to 7.7×10^{-5} only. This answers our question about how close to Δ_2 would be the formula (32), with h_2 and k_2 replaced H_2 and K_2 at $r = a - d$. In Fig. 2, g_r^δ is plotted as a function of depth between the surface and 1 km. The difference between g_r^δ and its linear fit is also plotted. It shows that the nonlinear part of g_r^δ is 10^8 to 10^9 times smaller than its linear part.

A more refined Earth model, which would include Earth rotation, ellipticity and lateral variations (Wahr 1981; Dehant & Ducarme 1987; Dehant *et al.* 1999), would probably give a more accurate estimate of the tidal gravity variations. But, a deformation of low harmonic degree is global and taking into account non-radial variations of the Earth's structure would not dramatically change the results we obtained for the tidal gravity variations and gravimetric factor of spherical models. They actually show that the depth dependence of the tidal gravity variation is almost as simple as it can be, that is a linear function of depth when the latter is small compared with the Earth radius. As a consequence, function Δ_2 is almost constant. This is the conclusion of this section.

In the next two sections, we investigate whether the difference of tidal gravity variations between the surface and 520 m under the surface can be detected with superconducting gravimeters.

4 CALIBRATION OF SUPERCONDUCTING GRAVIMETERS

In Section 5, we analyse the data provided by two superconducting gravimeters located at LSBB in Rustrel, France. The first one, the iOSG24, was installed in 2016 in a tunnel 520 m under the ground. The second one, the iGrav31, was installed in 2019 on the surface (Fig. 1).

Beforehand, we have to determine the calibration factors of the instruments. The calibration factor, or scale factor, of a gravimeter allows for the conversion of the output signal of the instrument, expressed in volt, into gravity variations, expressed in nm s^{-2}.

Two different types of calibration have been applied to the data of the iOSG24 and iGrav31. The first one is the classical calibration based on the simultaneous recording during up to a week by a FG5 absolute gravimeter running side by side with a superconducting gravimeter. The second one is a relative calibration of a superconducting gravimeter with respect to the other, at the same site and at the same distance from the centre of the Earth, by using two overlapped time series of usually one month but sometimes longer than one year.

The absolute calibration factors K_{abs} given in Table 2 were obtained with the help of the FG5 no. 206 operated by the Strasbourg team, except in 2021 when the Montpellier team operated the FG5 no. 202. The fractional errors for the absolute calibration factors are of the order of a few parts per thousand, ranging between 3.3 and

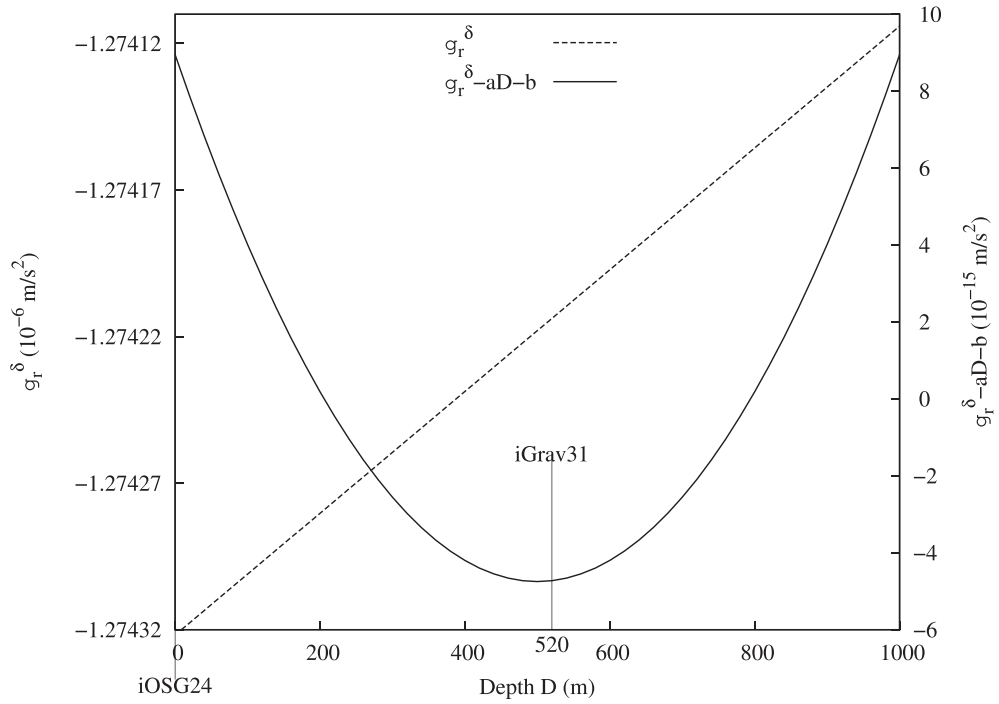

Figure 2. For the M_2 period of 12h25m14s and a slightly modified version of PREM, Lagrangian variation of gravity g_r^δ as a function of depth D and difference between g_r^δ and its linear fit $aD - b$, where $a = 2.07116 \times 10^{-13}$ s^{-2} and $b = 1.27432 \times 10^{-13}$ m s^{-2}. The nonlinear part of g_r^δ is 10^8 to 10^9 times smaller than its linear part.

Table 2. Absolute and relative calibration factors K_{Abs} and K_{Rel} for the iOSG24 and iGrav31. Each L1 and L2 norm adjustment value is given with its error. The numbers within parentheses are the fractional errors (in ‰), as explained in the text. The iGrav31 superconducting gravimeter has been calibrated at LSSB and at the J9 station near Strasbourg, France, whose location is shown in Fig. 1.

Superconducting gravimeter Location	Time (yr d)	Duration (d)	K_{Abs} (nm s^{-2}/V) L1 norm	K_{Abs} (nm s^{-2} V^{-1}) L2 norm	K_{Rel} (nm s^{-2} V^{-1})
iOSG24	2015 280	5	−451.7 ± 2.7 (6.0)	−451.6 ± 0.6 (1.3)	
Underground LSBB	2016 322	4	−451.6 ± 2.6 (5.8)	−452.6 ± 0.7 (1.5)	
	2019 291	2	−451.3 ± 2.9 (6.4)	−452.6 ± 0.7 (1.5)	
	2020 266	4	−451.1 ± 3.6 (8.0)	−450.5 ± 1.0 (2.2)	
	2021 153	6	−452.8 ± 1.5 (3.3)	−453.1 ± 1.2 (2.6)	
iGrav31	2019 297	6	−854.4 ± 4.3 (5.1)	−854.8 ± 1.7 (2.0)	
Surface LSSB	2020 272	5	−846.0 ± 7.4 (8.7)	−843.8 ± 3.1 (3.7)	
	2021 147	6	−853.2 ± 1.6 (1.9)	−853.6 ± 1.2 (1.4)	
iGrav31	2016 242	4	−852.8 ± 4.2 (4.9)	−853.7 ± 2.2 (2.6)	
J9 Strasbourg	2016 340	3	−859.0 ± 4.5 (5.2)	−857.8 ± 2.3 (2.7)	
	2017 94	2	−854.6 ± 7.6 (8.9)	−855.1 ± 3.6 (4.2)	−850.5 ± 0.1⋆ (0.12)
	2017 184	8	−854.0 ± 2.8 (3.3)	−853.2 ± 0.9 (1.1)	

Note. ⋆ Linear regression using a 30-d duration with 1 min samples by using the iOSG23 as a reference (−451 nm s^{-2} V^{-1}) at the station J9 in Strasbourg, France.

8.9×10^{-3} for the L1-norm calibration. Our results are in agreement with other studies on calibration with an absolute gravimeter, which show errors at the 10^{-3} level or a few parts in 10^{-4} (Hinderer *et al.* 1991; Francis & Van Dam 2002; Imanishi *et al.* 2002; Fukuda *et al.* 2005, 2021; Riccardi *et al.* 2011; Meurers 2012; Crossley *et al.* 2018).

The relative calibration factor K_{Rel} of the iGrav31 was obtained by a simultaneous recording in 2017 May with the iOSG23 installed at the station J9 near Strasbourg, France (Fig. 1), with the calibration factor -451 nm s^{-2} V^{-1} as a reference. The instruments were a few meters apart in the same building (Hinderer *et al.* 2022). A linear time regression on a 30-d duration record with 1 min samples was applied. The relative calibration uncertainty given in Table 2 is one order smaller than the absolute calibration uncertainties. This was also found in previous studies on relative calibration (Riccardi *et al.* 2011; Meurers 2012; Hinderer *et al.* 2022). However, the scale factor of the iGrav31 probably changed when it was warmed up to room temperature to be transported to the LSBB in Rustrel. The stability of calibration factors due to re-levitation or transportation of iGravs is discussed by Schäfer *et al.* (2020) and Hinderer *et al.* (2022).

The absolute calibration factors of the iOSG24 and iGrav31 are shown in Fig. 3. The average values of the absolute calibration factors for the two superconducting gravimeters are given in Table 3. The average values using the L1 and L2 norms agree within the error bars. The L2-norm estimate provides larger error bars than the L1-norm estimate, although the L1-norm error bars of individual calibration values are larger because of the outliers in absolute gravimeter drop estimates. Actually, the scatter of the L1-norm estimates of the calibration factors is smaller, which gives a weighted average value with a smaller uncertainty.

Now knowing the calibration factors of the two superconducting gravimeters installed at the LSBB, we can proceed with the analysis of the tidal gravity variations, both on and under the surface.

5 OBSERVED TIDAL GRAVITY VARIATIONS AT THE SURFACE AND UNDERGROUND

As can be calculated from the geographical coordinates of the LSBB stations given in the caption of Fig. 1, the horizontal, latitudinal and longitudinal distances between the instruments are 90.1, 57.6 and 70.4 m, respectively. Before we launch into the analysis of the data provided by the two instruments, we have to compare the latitudinal tidal gravity variation to the vertical one. The fractional tidal gravity variation due to latitude differences is the fractional difference between the degree 2, order 2 associated Legendre function evaluated at the two locations, that is 1.8×10^{-5}. This is 5–10 times smaller than our theoretical estimates of the corresponding vertical ratio, so we can safely ignore it.

The signals $g^{\delta}_{\mathrm{iGrav31}}$ and $g^{\delta}_{\mathrm{iOSG24}}$ simultaneously recorded during 471 d between 2019 and 2021 by the superconducting gravimeters located respectively on the surface and 520 m under the surface are plotted in Figs 4(a) and (b). Being largely dominated by the tidal gravity variations, they look very similar. The iOSG24 recording shows some short gaps due to different problems affecting the instrument chain. The gaps are filled with the local tide calculated on the basis of the tidal parameters, namely the gravimetric factor and phase, estimated by a tidal analysis conducted on the entire available data set.

The difference $g^{\delta}_{\mathrm{iGrav31}} - g^{\delta}_{\mathrm{iOSG24}}$ displayed in Fig. 4(c) mainly contains a residual long-term drift and a mostly annual residual signal, the latter being related to the gravity effect of the time-variable hydrological contribution of the water distribution inside the Fontaine de Vaucluse catchment (Kumar *et al.* 2023). If the fractional difference $(g^{\delta}_{\mathrm{iGrav31}} - g^{\delta}_{\mathrm{iOSG24}})/g^{\delta}_{\mathrm{iGrav31}}$ for the M_2 tide was 8.47×10^{-5}, as we found for PREM in Section 3, and if we take as surface gravity variation the signal $g^{\delta}_{\mathrm{iGrav31}}$, the difference $g^{\delta}_{\mathrm{iGrav31}} - g^{\delta}_{\mathrm{iOSG24}}$ would be given by Fig. 4(d). Its maximum absolute value is smaller than 0.15 nm s^{-2}, which is to be compared to the maximum absolute value of the actual difference shown in Fig. 4(c), which peaks at 300 nm s^{-2}.

To detect elusive differences between the tidal signals from the two superconducting gravimeters, we focus on one of the largest tidal component in the semi-diurnal band at the latitude of Rustrel, namely the M_2 tide. Considering minor waves in the semi-diurnal band would not provide significantly different results. Moreover, a smaller wave such as S_2 could probably be affected by thermal and baro-thermal effects, which would be different at the surface and 520 m below. For a similar reason, we do not search for the diurnal K_1 tide that, although larger than the M_2 tide, is spectrally very close to the thermal band and could therefore be contaminated by the S_1 solar wave.

To isolate the M_2 frequency band, from 1.931 to 1.934 cycle per day (cpd), we first filter the data with two low-pass fast Fourier transform (FFT) filters with bandwidth 0.01 cpd and cut-off frequencies 1.91 and 1.96 cpd. This is equivalent to a passband filter having as corner frequencies 1.91 and 1.96 cpd. In contrast to time-domain filters, such as the Infinite Impulse Response filter or the Finite Impulse Response filter, the FFT filter is based on manipulating specific frequency components of a signal. It consists in taking the Fourier transform of the signal, then attenuating or amplifying specific frequencies and finally inversely transforming the result. It is particularly suitable for extracting the low peaks of signals where large harmonics are present nearby; in such a case, time-domain filters would fail (Oppenheim & Schafer 2014). This bandpass filtering also allows for minimizing the non-tidal influences that may vary according to the location of the instrument. This is especially true for solar radiation, hydrology and long-term instrumental drift. To test the efficiency of the filter used to extract the M_2 signal, it is applied to both the raw and filtered data of a 10-yr time-series of synthetic tides. The amplitude spectra shown in Fig. 5(a) confirm that the M_2 tidal signal is correctly filtered.

Next, we identically apply the filtering procedure to both the iOSG24 and iGrav31 data. By the way, we obtain amplitude spectra in full agreement with the amplitude found by a least-square adjustment of the M_2 wave using the time signals. We then subtract the filtered signals from each other. Apart from small amplitude secondary waves, which are still present in the M_2 band, the difference between the filtered signals of the two gravimeters is dominated by the M_2 wave. Again, the M_2 spectral amplitude is similar to the one we find when we apply, without any filtering, the FFT to the difference $g^{\delta}_{\mathrm{iGrav31}} - g^{\delta}_{\mathrm{iOSG24}}$.

It is worth noting it would be pointless to run a tidal analysis software like ETERNA-X (Schüller 2020) that fits the time signal to a series of sinusoids at the tidal frequencies. Indeed, in ETERNA-X or similar codes, it is assumed that gravity is measured at the Earth's surface, even if the elevation above the ellipsoid can be adjusted. This means that the masses between an underground station and the surface are not taken into account.

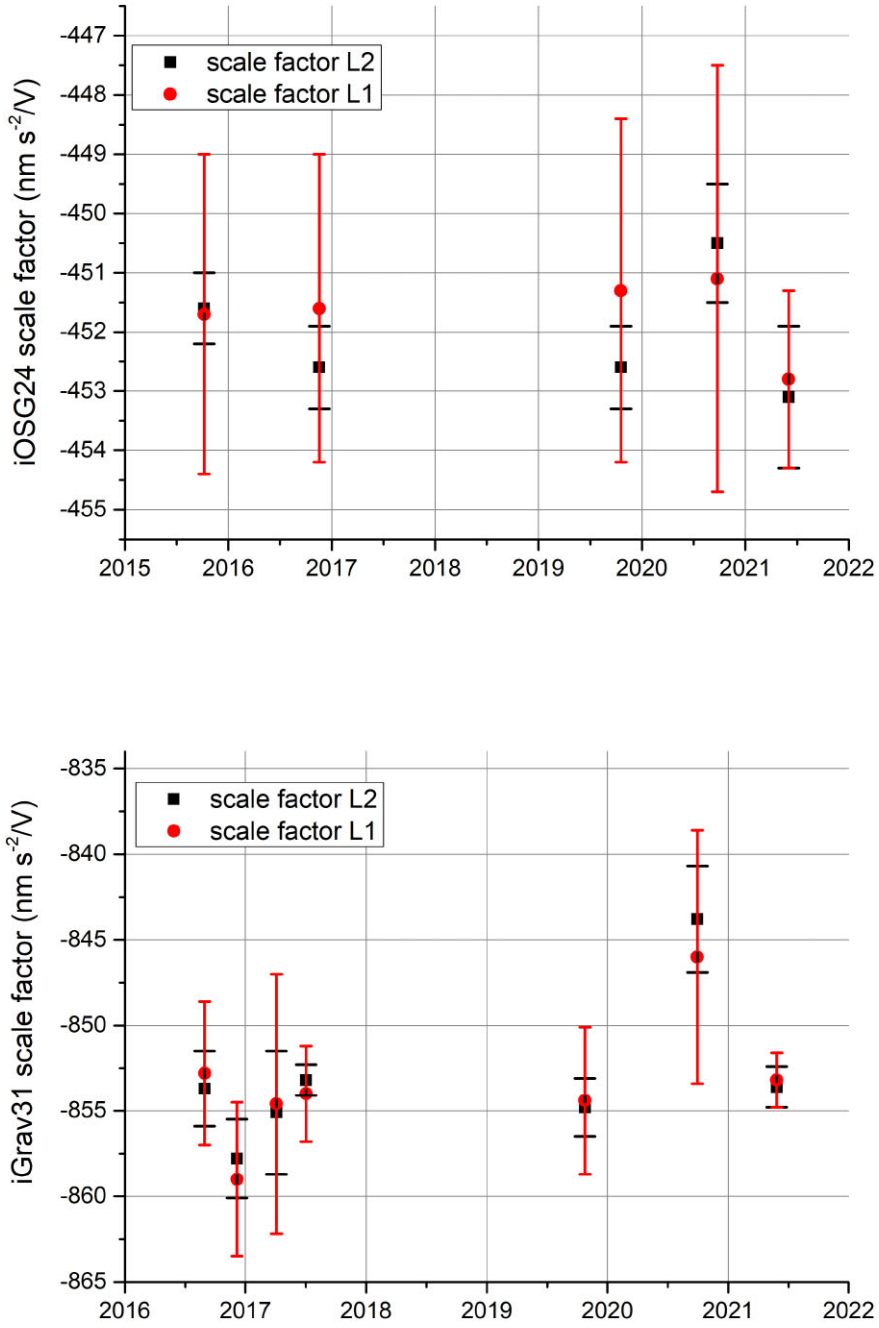

Figure 3. L1- and L2-norm estimates of absolute scale factor K_{Abs}^{iOSG24} (top) and $K_{Abs}^{iGrav31}$ (bottom) at LSBB. In chronological order, the number of days of the simultaneous recording was 5, 4, 2, 4, 5 for the iOSG24 and 4, 3, 2, 8, 6, 5, 6 for the iGrav31.

Table 3. Average values of absolute calibration factors K_{Abs}, in nm s^{-2} V^{-1}.

Superconducting gravimeter	L1 norm	L2 norm
iGrav31	−853.7±0.7	−853.5 ± 1.5
iOSG24	−451.6 ± 0.3	−452.1 ± 1.1

To highlight amplitude discrepancies between spectra, the difference between the filtered signals of the iGrav31 and iOSG24 is calculated for three different calibration factors of the iGrav31. The amplitude spectra are shown in Figs 5(b)–(d). First, we consider the scale factor coming from the relative calibration performed with the iOSG23 at the station J9 in Strasbourg (Table 2 and Fig. 5b). Second, we consider the scale factors retrieved from L1 and L2-norms linear regression with FG5 absolute gravity measurements (Table 3, and Figs 5c and d). All the spectra are normalized with respect to the amplitude of the M_2 tide at the LSBB, which is 449.2 nm s^{-2}.

The red error bars, named fractional errors to shorten the expression 'fractional calibration errors', are obtained in the following way. In the case of relative calibration, the fractional calibration error only comes from the regression since the scale factor of the reference gravimeter, the iOSG23, is assumed to be not affected by error. As the numbers within parentheses in the last column of Table 2, it is simply given by $\sigma_{Rel}^{iGrav31}/K_{Rel}^{iGrav31}$, where $\sigma_{Rel}^{iGrav31}$ is the

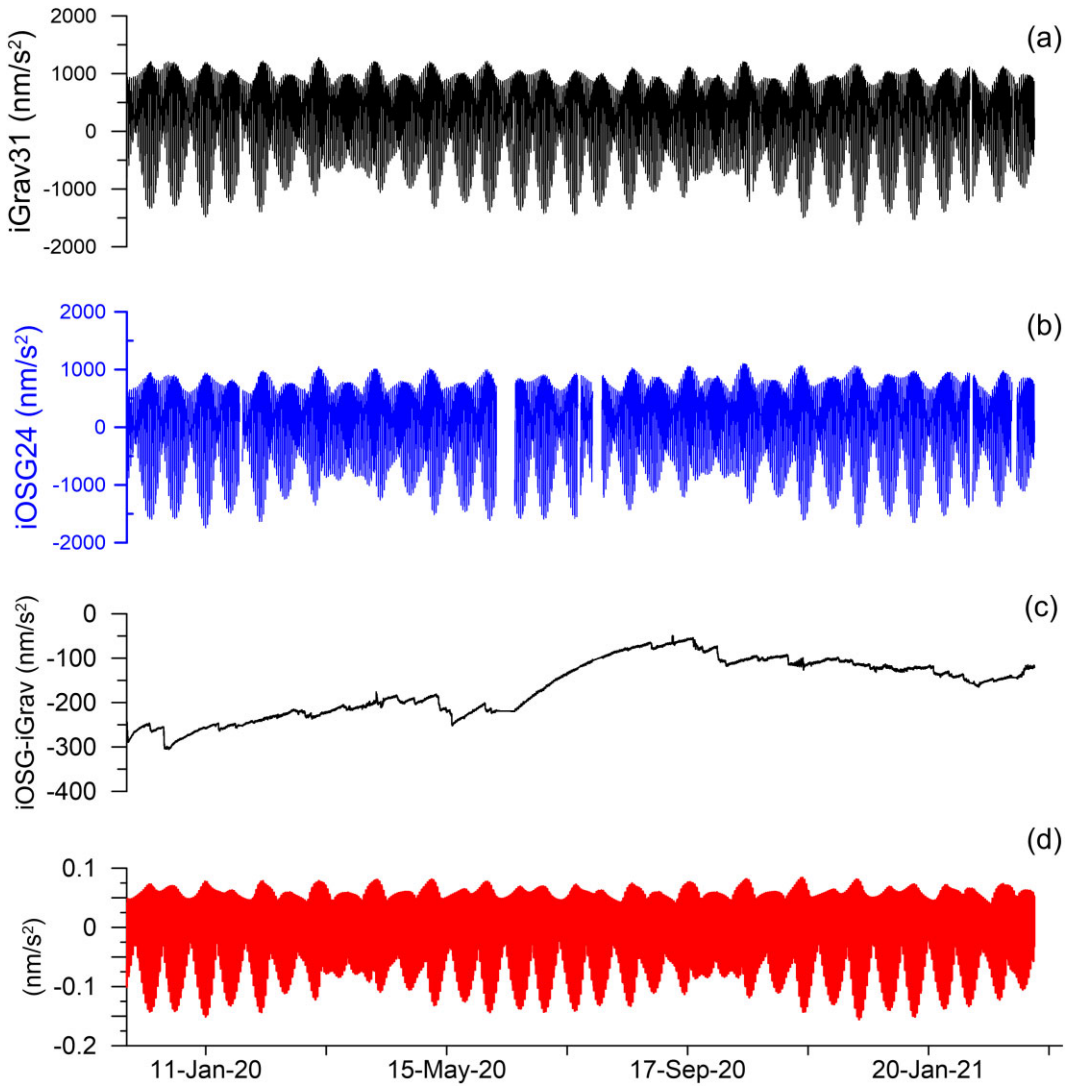

Figure 4. Gravity data at LSBB. (a) $g^{\delta}_{\mathrm{iGrav31}}$ raw data, (b) $g^{\delta}_{\mathrm{iOSG24}}$ raw data, (c) actual difference $g^{\delta}_{\mathrm{iGrav31}} - g^{\delta}_{\mathrm{iOSG24}}$ and (d) hypothetical difference $g^{\delta}_{\mathrm{iGrav31}} - g^{\delta}_{\mathrm{iOSG24}}$ based on the assumption that the surface gravity variation is $g^{\delta}_{\mathrm{iGrav31}}$ and that the ratio $(g^{\delta}_{\mathrm{iGrav31}} - g^{\delta}_{\mathrm{iOSG24}})/g^{\delta}_{\mathrm{iGrav31}}$ is PREM's, that is 8.47×10^{-5}.

error associated to the relative calibration factor. In the case of absolute calibration, one has to account for the calibration error of the two gravimeters, which leads to a fractional calibration error equal to $\sqrt{(\sigma^{\mathrm{iGrav31}}_{\mathrm{Abs}}/\mathrm{K}^{\mathrm{iGrav31}}_{\mathrm{Abs}})^2 + (\sigma^{\mathrm{iOSG24}}_{\mathrm{Abs}}/\mathrm{K}^{\mathrm{iOSG24}}_{\mathrm{Abs}})^2}$, where the σs and Ks are provided in Table 3.

As expected, the spectra obtained with the absolute scale factors of the iGrav31 display larger amplitudes (Figs 5c and d) than the spectrum obtained by calibrating the iGrav31 relatively to the iOSG23 in Strasbourg (Fig. 5b). The relative calibration aims at making the difference between the two signals as small as possible. It is not exactly zero mainly because the relative scale factor is obtained by using all the tidal components, not only the M_2 wave. The relative calibration factor leads to the largest amplitude difference for the M_2 tidal wave. However, as mentioned in Section 4, the scale factor of the iGrav31 may have changed when it was moved from Strasbourg to the LSBB in Rustrel.

The normalized amplitude of the spectra is of order 10^{-3}. Hence, it is smaller than the confidence interval, which is twice the fractional error, except in Fig. 5(b) where we used the relative scale factor found at J9. However, as we have just seen above, it might not be appropriate to use this relative scale factor at the LSBB.

The spectra clearly show that inaccuracies of calibration are larger than the predicted fractional difference, 8.47×10^{-5}, between the tidal gravity variations at the surface and 520 m under the surface of PREM, making it undetectable. Therefore, a conclusion of our analysis is that one of the fundamental limits to the possibility of detecting a difference in the tidal signals of such small amplitude, smaller than 0.1 nm s^{-2}, is the accuracy of the calibration. Our only metrologically meaningful calibrations are the absolute ones, but the fractional errors we obtain are 0.0011 and 0.003 according to the L1 or L2 norm, respectively, Relative calibration only makes sense if it is done with the two gravimeters installed side by side, measuring the same gravity variations (Hinderer *et al.* 2022). The

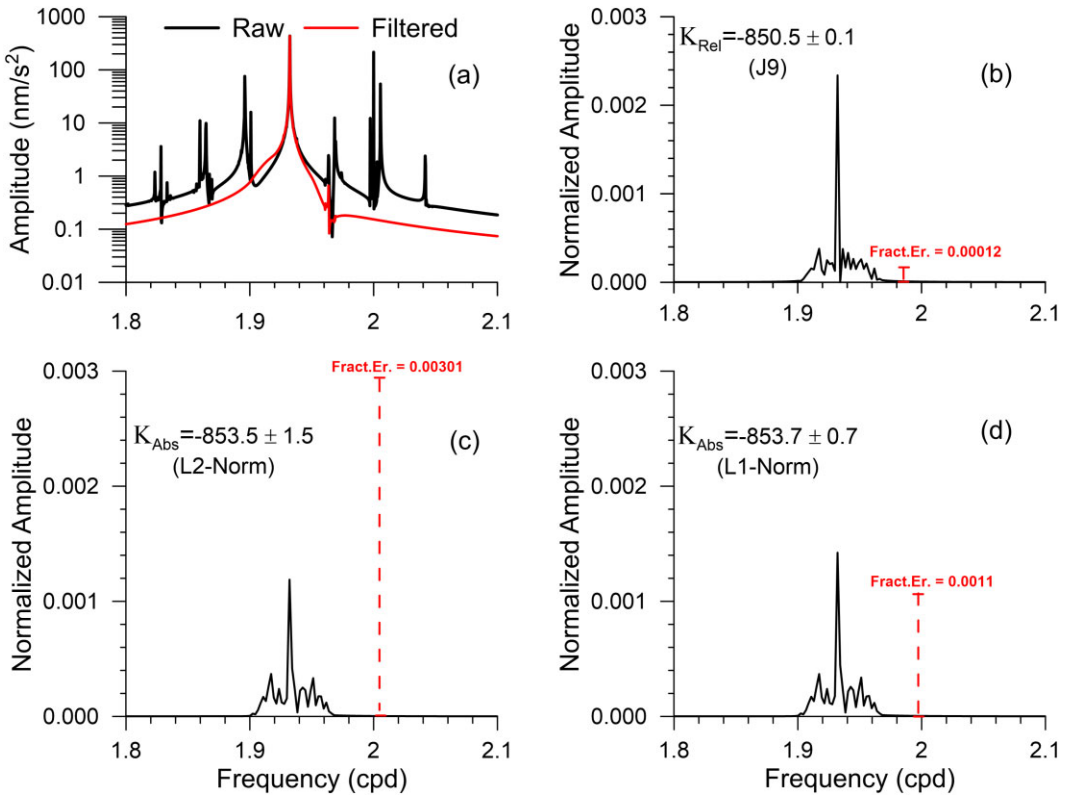

Figure 5. Spectral analysis of the gravity data at LSBB shown in Fig. 4. (a) Check of the efficiency of the filter used to extract a frequency signal centred in the M_2 tidal band: spectra of a 10-yr synthetic raw and filtered (the smoothest curve) tidal signal; (b)–(d) normalized amplitude spectrum of the bandpass filtered difference for three scale factors of the iGrav31 denoted by K_{Rel} and K_{Abs} and expressed in nm s^{-2} V^{-1} in the insets and given in Tables 2 and 3; the normalizing factor is the amplitude of the M_2 tide at the LSBB, which is 449.2 nm s^{-2}. The fractional calibration error, which can be obtained from the data in Tables 2 and 3 as explained in the text, is plotted as a dashed vertical line.

smallest error bar, 1.2×10^{-4}, is from the J9 relative calibration experiment, but obviously the scale factor may have changed when the iGrav31 was moved from J9 to the LSBB. Even in this case the error bar would be too large to detect the predicted tidal difference between the underground and surface sites.

6 CONCLUSION

We have theoretically and observationally investigated the difference between the tidal gravity variations on the surface and 520 m under the surface at the Low Noise Underground Laboratory (LSBB = Laboratoire Souterrain à Bas Bruit) in Rustrel, France.

Analytical modelling with homogeneous and incompressible spherical Earth models has shown that the Lagrangian variation of gravity due to tidal forces is strictly a linear function of depth when the model is fluid. Analytical modelling with a homogeneous and incompressible solid Earth model and numerical modelling with a realistic Earth model have shown that the Lagrangian variation of gravity due to tidal forces is only approximately a linear function of depth. Given the smallness of both the depth and the Lagrangian tidal variation of gravity, the linear approximation is sufficient, providing a fractional difference of semi-diurnal tidal gravity variation of 8.5×10^{-5} between the surface and the 520-m depth.

Gravity variations have been measured at LSBB between 2019 and 2021 simultaneously with two models of superconducting gravimeters. The first one, the iOSG24, is installed 520 m under the surface. The second one, the iGrav31, is installed on the surface and horizontally distant by 90.1 m from the iOSG24. Both instruments have been calibrated at their installation sites with absolute gravimeters. Calibration of the iGrav31 relative to the iOSG23 at the station J9 near Strasbourg has also been made.

The raw data of the gravimeters have been FFTed in the semi-diurnal M_2 band. Then the difference between the two FFTs has been computed. The process has been repeated three times by using various estimates of the iGrav31 calibration factor. We found that the uncertainties associated to the calibration factors are too large to allow for the detection of a difference between the semi-diurnal tidal variations at the surface and at a 520-m depth as small as what was theoretically predicted.

With the same limitation due to the calibration factors, and assuming a linear downward extrapolation of the tidal gravity variation, the difference between the tidal signals would be observable if the underground gravimeter was installed 4–5 km from the surface. Presently, such an experiment is, however, not feasible. In addition to logistic problems due to the size of the superconducting gravimeters, the increase of temperature with depth is another limiting factor. Indeed, superconducting gravimeters need to be continuously cooled by using a helium compressor. But this device does not work at temperatures above 308 K. Given that most geothermal gradients are approximately 25 K km^{-1}, the depth where one could plan to install a superconducting gravimeter is thus strongly limited. Although mechanical borehole gravimeters of reduced size exist (Jiaming et al. 2011), their precision, of the order of 10 nm s^{-2}, would be by far too low in comparison to the one of superconducting gravimeters such as those used in this study. The same hold for

the microelectromechanical system gravimeters (Middlemiss *et al.* 2016).

ACKNOWLEDGMENTS

We thank Walter ZÜRN for a careful review of a first draft of the paper. We gratefully acknowledge numerous fruitful discussions with our late friend and colleague Hilaire LEGROS. The iGrav31 was funded by Equipex CRITEX (Study of the critical zone) ANR-11-EQPX-0011 (https://www.critex.fr). The iOSG24 was funded by the Equipex MIGA (Matter wave-laser based Interferometer Gravitation Antenna) ANR-11-EQPX-0028 (http://miga-project.org).

DATA AVAILABILITY

The iOSG24 data are available from the IGETS database http://igets.u-strasbg.fr at the address https://doi.org/10.5880/igets.ru.l1.001. The iGrav31 data belong to the research project EQUIPEX CRITEX (https://www.critex.fr) dedicated to hydrological investigations. Originally, the recording was only meant to be of limited duration. Hence, the data are not uploaded to the IGETS database. They are available upon request to the corresponding author.

REFERENCES

Alterman, Z., Jarosch, H. & Pekeris, L., 1959. Oscillations of the Earth, *Proc. Roy. Soc. Lond., Ser. A,* **252,** 80–95. doi: 10.1098/rspa.1959.0138.

Bierson, C.J., 2024. The impact of rheology model choices on tidal heating studies, *Icarus,* **414,** 116026. doi:10.1016/j.icarus.2024.116026.

Bromwich, T.J.I'A., 1899. On the influence of gravity on elastic waves, in particular, on the vibrations of an elastic globe, *Proc. London Math. Soc.,* **30,** 98–120.

Calvo, M., 2015. *Analysis of long-term gravity records in Europe; Consequences for the retrieval of small amplitude and low frequency signals including the Earth's core resonance,* PhD thesis, Universidad Complutense de Madrid, Université de Strasbourg.

Crossley, D., Calvo, M., Rosat, S. & Hinderer, J., 2018. More thoughts on AG-SG comparisons and SG scale factor determinations, *Pure appl. Geophys.,* **175**(5), 1699–1725.

Dahlen, F.A. & Tromp, J., 1998. *Theoretical Global Seismology,* Princeton University Press, Princeton, NJ.

Dehant, V. & Ducarme, B., 1987. Comparison between the theoretical and observed gravimetric factors, *Phys. Earth planet. Inter.,* **49,** 192–212. doi: 10.1016/0031-9201(87)90022-7.

Dehant, V., Defraigne, P. & Wahr, J.M., 1999. Tides for a convective Earth, *J. geophys. Res.,* **104**(B1), 1035–1058.

Dziewonski, A. & Anderson, D., 1981. Preliminary reference Earth model, *Phys. Earth planet. Inter.,* **25,** 297–356. doi: 10.1016/0031-9201(81)90046-7.

Francis, O. & Van Dam, T., 2002. Evaluation of the precision of using absolute gravimeters to calibrate superconducting gravimeters, *Metrologia,* **39,** 485–488. doi: 10.1088/0026-1394/39/5/9.

Fukuda, Y., Iwano, S., Ikeda, H., Hiraoka, Y. & Doi, K., 2005. Calibration of the superconducting gravimeter CT#043 with an absolute gravimeter FG5#210 at Syowa Station, Antarctica, *Polar Geosci.,* **18,** 41–48.

Fukuda, Y., Okuno, J., Doi, K. & Lee, C.-K., 2021. Gravity observations at Jang Bogo Station, Antarctica, and scale factor calibrations of different relative gravimeters, *Polar Sci.,* 100702, doi:10.1016/j.polar.2021.100702.

Hinderer, J., Crossley, D. & Warburton, R.J., 2015. Superconducting gravimetry, in *Treatise on Geophysics,* pp. 59–115, Elsevier. doi: 10.1016/B978-0-444-53802-4.00062-2.

Hinderer, J., Florsch, N., Mäkinen, J., Legros, H. & Faller, J.E., 1991. On the calibration of a superconducting gravimeter using absolute gravity measurements, *Geophys. J. Int.,* **106,** 491–497. doi: 10.1111/j.1365-246X.1991.tb03907.x.

Hinderer, J. & Legros, H., 1989. Elasto-gravitational deformation, relative gravity changes and Earth dynamics, *Geophys. J. Int.,* **97,** 481–495. doi: 10.1111/j.1365-246X.1989.tb00518.x.

Hinderer, J. *et al.*, 2022. Intercomparing superconducting gravimeter records in a dense meter-scale network at the J9 gravimetric observatory of Strasbourg, France, *Pure appl. Geophys.,* **179,** 1701–1727. doi: 10.1007/s00024-022-03000-4.

Imanishi, Y., Higashi, T. & Fukuda, Y., 2002. Calibration of the superconducting gravimeter T011 by parallel observation with the absolute gravimeter FG5 #210: a Bayesian approach, *Geophys. J. Int.,* **151,** 867–878. doi: 10.1046/j.1365-246X.2002.01806.x.

Jiaming, L., Zhigui, Y., Xingwei, W., Ping, G. & Jin, W., 2011. A high-precision borehole gravimeter, *Geod. Geodyn.,* **2**(3), 76–79.

Kellogg, O.D., 1953. *Foundations of Potential Theory,* Dover, New York.

Kumar, S., Rosat, S., Hinderer, J., Mouyen, M., Boy, J.-P. & Israil, M., 2023. Delineation of aquifer boundary by two vertical superconducting gravimeters in a karst hydrosystem, France, *Pure appl. Geophys.,* **180,** 611–628. doi: 10.1007/s00024-022-03186-7.

Love, A.E.H., 1909. The yielding of the earth to disturbing forces, *Proc. R. Soc. Lond. A.,* **82,** 73–88.

Meurers, B., 2012. Superconducting gravimeter calibration by colocated gravity observations: Results from GWR C025, *Int. J. Geophys.,* **954271,** 1–12. doi: 10.1155/2012/954271.

Middlemiss, R.P., Samarelli, A., Paul, D.J., Hough, J., Rowan, S. & Hammond, G.D., 2016. Measurement of the earth tides with a MEMS gravimeter, *Nature,* **531,** 614–617. doi: 10.1038/nature17397.

Oppenheim, A.V. & Schafer, R.W., 2014. *Discrete-Time Signal Processing,* 3rd edn, Pearson Education Limited.

Peale, S.J. & Canup, R.M, 2015. The origin of the natural satellites, in *Treatise on Geophysics,* 2nd edn, Vol. **10,** pp. 559–604. Elsevier B.V. doi: 10.1016/B978-0-444-53802-4.00177-9.

Rambaux, N. & Castillo-Rogez, J., 2013. Tides on satellites of giant Planets, In *Tides in Astronomy and Astrophysics,* Souchay, Mathis & Tokieda(eds.), pp. 167–200. Springer-Verlag, Heidelberg.

Riccardi, U., Rosat, S. & Hinderer, J., 2011. On the accuracy of the calibration of superconducting gravimeters using absolute and spring sensors: a critical comparison, *Pure appl. Geophys.,* **169**(8), 1343–1356.

Rogister, Y., 1995. Static deformations of incompressible Earth models, *Acta Geod. Geophys. Hungarica,* **30,** 153–161.

Rosat, S. *et al.*, 2018. A two-year analysis of the iOSG24 superconducting gravimeter at the low noise underground laboratory (LSBB URL) of Rustrel, France: Environmental noise estimate, *J. Geodyn.,* **119,** 1–8. doi: 10.1016/j.jog.2018.05.009.

Schäfer, F. *et al.*, 2020. Performance of three iGrav superconducting gravity meters before and after transport to remote monitoring sites, *Geophys. J. Int.,* **223,** 959–972. doi: 10.1093/gji/ggaa359.

Schüller, K., 2020. Theoretical basis for Earth tide analysis and prediction, *Manual-01-ET34-X-V80,* 217. Surin, Thailand.

Sénéchal, G., Rousset, D. & Gaffet, S., 2013. Ground Penetrating Radar investigation inside a karstified limestone reservoir, *Near Surf. Geophys.,* **11**(3), 283–291.

Thomson, W., 1863a. On the rigidity of the Earth, *Phil. Trans. R. Soc.,* **153,** 573–582.

Thomson, W., 1863b. Dynamical problems regarding elastic spheroidal shells and spheroids of incompressible liquid, *Phil. Trans. R. Soc.,* **153,** 583–616.

Torge, W., 1989. *Gravimetry,* de Gruyter: New York.

Wahr, J.M., 1981. Body tides on an elliptical, rotating, elastic and oceanless earth, *Geophys. J. R. astr. Soc.,* **64,** 677–703. doi: 10.1111/j.1365-246X.1981.tb02690.x.

Wenzel, H.-G., 1997. Tide-generating potential for the Earth, In: *Tidal Phenomena,* Wilhelm, Zürn & Wenzel(eds.), pp. 9–26 Springer-Verlag, Berlin.

Wilhelm, H., Zürn, W. & Wenzel, H.-G., 1997. *Tidal Phenomena,* Springer-Verlag, Berlin. doi: 10.1007/BFb0011453.

APPENDIX A: DYNAMIC LOVE NUMBERS AND GRAVIMETRIC FACTOR OF INCOMPRESSIBLE HOMOGENEOUS EARTH MODELS

Let us consider a spherical homogeneous incompressible fluid Earth model that is subjected to a tidal deformation. By solving the equations of motion (Alterman *et al.* 1959), one finds that the radial displacement $u_r(r)$ of harmonic degree ℓ varies as

$$u_r(r) \sim r^{\ell-1} \tag{A1}$$

and that $\phi^{\Delta\,\mathrm{in}}(r)$ varies as r^ℓ [eq. (35)]. The Love numbers are found to be

$$h_\ell = \frac{1}{\frac{2(\ell-1)}{2\ell+1} - \frac{\mathfrak{m}}{\ell}} \tag{A2}$$

and

$$k_\ell = \frac{3}{2\ell+1} h_\ell, \tag{A3}$$

where $\mathfrak{m}$ is the dimensionless parameter defined by

$$\mathfrak{m} = \frac{\omega^2 a}{g(a)}. \tag{A4}$$

For $\rho = 5515$ kg m^{-3}, $a = 6371$ km, $\ell = 2$ and a semi-diurnal tide, we have $g(a) = 9.81$ m s^{-2}, $\mathfrak{m} = 1.3738 \times 10^{-2}$, $h_2 = 2.5439$, $k_2 = 1.5263$ and $\delta_2 = 1.2544$.

We notice that eq. (A3) is consistent with eq. (37) and that h_ℓ and k_ℓ tend to infinity when

$$\omega^2 = \frac{2\ell(\ell-1)}{2\ell+1}\frac{g(a)}{a}. \tag{A5}$$

ω is then an eigenfrequency of the model (Thomson 1863b). For $\ell = 2$, the corresponding eigenperiod is approximately 94 min and is therefore significantly smaller than the tidal periods, so that we can assert that there could be no resonance phenomenon.

With relation (38) and the Love number h_ℓ given by eq. (A2), we find

$$\delta_\ell = 1 + \frac{(\ell--1)}{\ell(2\ell+1)} h_\ell = \frac{\ell--1--\mathfrak{m}}{\ell} h_\ell = \frac{(2\ell+1)(\ell-1-\mathfrak{m})}{2\ell(\ell-1)-\mathfrak{m}(2\ell+1)}. \tag{A6}$$

The specific static case, that is, $\mathfrak{m} = 0$, was studied by Rogister (1995).

Let us now assume that the homogeneous incompressible Earth model is solid with rigidity μ. Then, $u_r(r)$ is given by (Bromwich 1899)

$$u_r(r) = C_1 \left(\frac{r}{a}\right)^{\ell-1} + C_2 \frac{j_\ell(x)}{x}, \tag{A7}$$

where C_1 and C_2 are constants, $j_\ell(x)$ is the spherical Bessel function of the first kind of order ℓ,

$$x = x(r) = \kappa r \tag{A8}$$

and

$$\kappa^2 = \frac{\rho\omega^2}{\mu}. \tag{A9}$$

The behaviour of $j_\ell(x)$ when x is small is

$$\lim_{x\to 0} j_\ell(x) = \frac{x^\ell}{(2\ell+1)!!}, \tag{A10}$$

where $(2\ell+1)!! = (2\ell+1)(2\ell-1)(2\ell-3)\ldots$ With this approximation, both terms of $u_r(r)$ in eq. (A7) are proportional to $r^{\ell-1}$ and, therefore, $u_r(r) \sim r^{\ell-1}$ as in the liquid case. Let us see if the approximation is sufficiently accurate. We take $\rho = 5515$ kg m^{-3} and $\mu = 1.46 \times 10^{11}$ Pa. The maximum of κr is at the surface $r = a$. For $\ell = 2$ and a semi-diurnal tide, we have $\kappa a = 0.18058740$. Since

$$j_2(x) = \left(\frac{3}{x^3} - -\frac{1}{x}\right)\sin x - -\frac{3}{x^2}\cos x, \tag{A11}$$

we obtain, with 10 significant digits, $j_2(\kappa a) = 2.169060709\ 10^{-3}$. The same accuracy can be achieved if we expand $j_2(x)$ in the following way:

$$j_2(x) \simeq \frac{x^2}{15} - -\frac{x^4}{210} + \frac{x^6}{7560} - -\frac{x^8}{518400}. \tag{A12}$$

Keeping only the first three terms in eq. (A12) provides a 8-digit accuracy, keeping only the first two terms provides a 5-digit accuracy, and the quadratic approximation, a 3-digit accuracy. This shows that, for $\ell = 2$, $u_r(r)$ is only very approximately a linear function of r. Using the approximation (A12) for $j_2(x)$, we obtain the degree-2 Love number

$$h_2 \simeq \frac{5}{2}\left\{1 + \frac{19\mu}{2\rho g(a)a}\left[1 - \frac{79}{570}x^2(a) - \frac{143}{410400}x^4(a)\right]\right\}^{-1}. \tag{A13}$$

Eqs (37) and (38), which rely on $u_r(a)$ but not on the r-dependence of u_r, remain valid in the solid case. Therefore, k_2 and δ_2 are still given by

$$k_2 = \frac{3}{5} h_2 \tag{A14}$$

and

$$\delta_2 = 1 + \frac{h_2}{10}. \tag{A15}$$

For a semi-diurnal tide, we have $h_2 = 0.4997$, $k_2 = 0.2998$ and $\delta_2 = 1.04997$. When $\omega = 0$ and, consequently, $x = 0$, one recovers Thomson's (1863a) exact static solution.